Supplement of The Cryosphere, 20, 6309–6329, 2026
https://doi.org/10.5194/tc-20-6309-2026-supplement
© Author(s) 2026. CC BY 4.0 License.



The Cryosphere Open Access EGU

Supplement of

Identifying Snow-Covered Areas from Unoccupied Aerial Systems (UAS) Visible Imagery and Lidar: A Comparison of Methods

Mahsa Moradi et al.

Correspondence to: Mahsa Moradi (mm1631@usnh.edu)

The copyright of individual parts of the supplement might differ from the article licence.

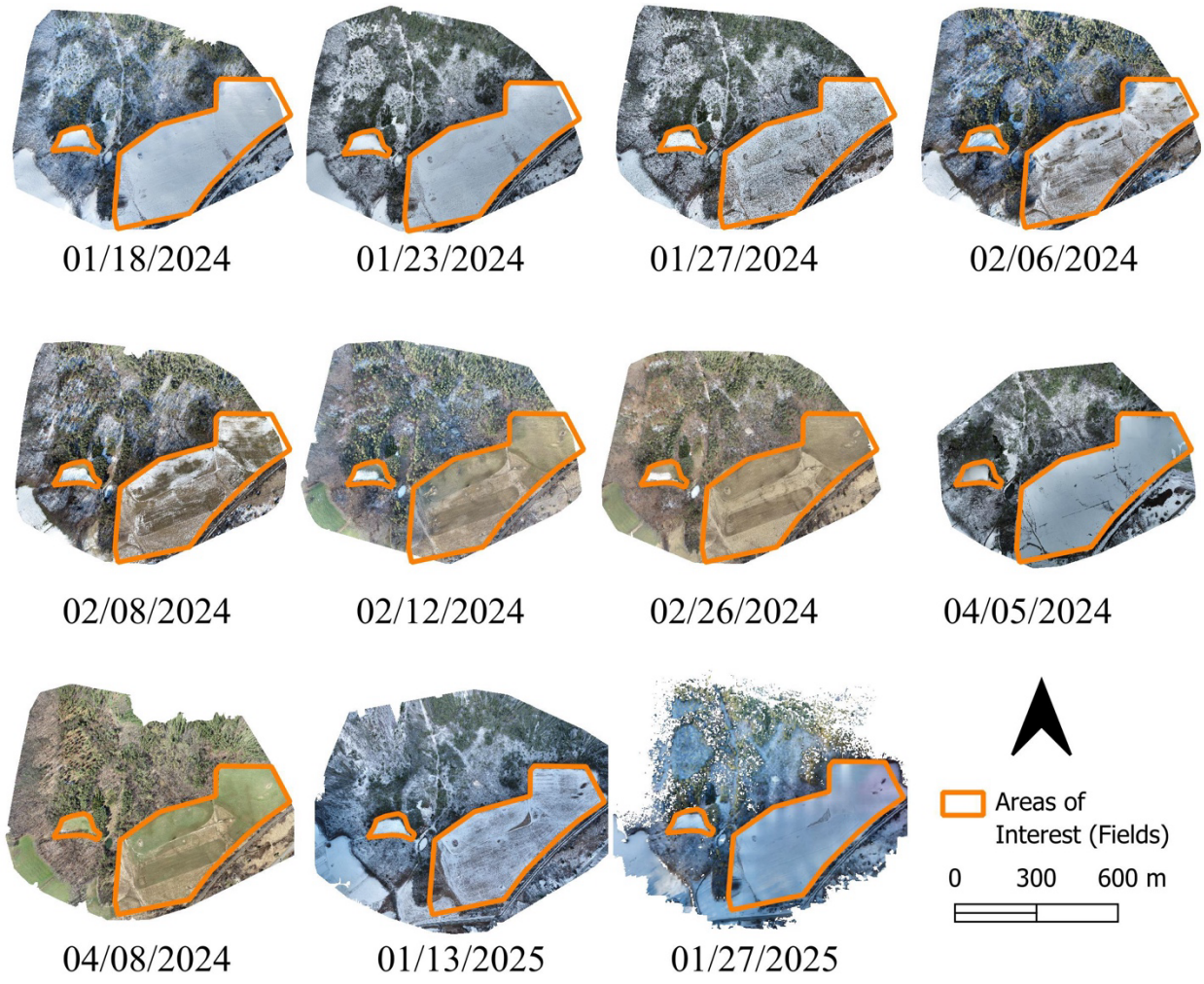


Figure S1. RGB orthomosaics of Kingman Farm acquired with the Phantom 4. Survey dates are shown below each orthomosaic. Areas of interest are outlined in orange.

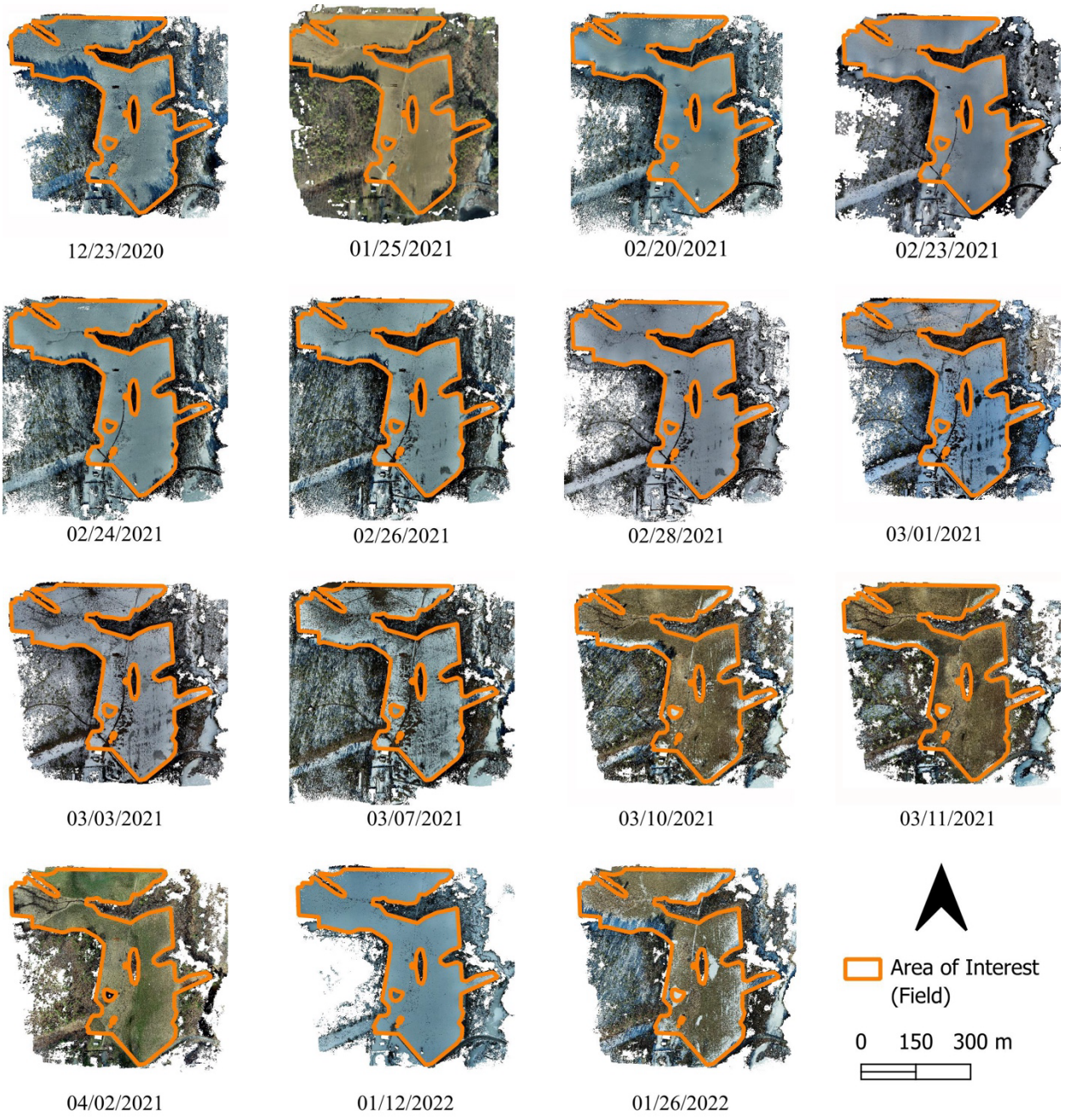


Figure S2. RGB orthomosaics of Thompson Farm acquired with the Phantom 4. Survey dates are shown below each orthomosaic. Areas of interest are outlined in orange.

Estimating Sky Coverage:

The clearness index (K_c) was computed as the ratio between observed shortwave radiation and the estimated clear-sky value:

$$K_c = \frac{SW_{obs}}{SW_{clear}} \quad \text{(S1)}$$

Table S1. Estimated sky condition based on clearness index

Clearness index	Sky Condition
$0.85 < K_c$	Clear
$0.60 < K_c \leq 0.85$	Mostly Clear
$0.35 < K \leq 0.60$:	Partly Cloudy
$K_c \leq 0.35$	Cloudy

To estimate the theoretical clear-sky incoming shortwave radiation (SW_{clear}) at the surface, we used a simplified atmospheric transmissivity model that accounts for solar geometry, time of year, and geographic location. The clear-sky incoming shortwave radiation (W/m^2) at a given time and location was estimated as:

$$SW_{clear} = S_0 \times \cos(\theta) \times \tau \quad \text{(S2)}$$

where S_0 is the top-of-atmosphere solar irradiance (W/m^2), $\cos(\theta)$ is the cosine of the solar zenith angle, and τ is an empirical atmospheric transmissivity factor (set to 0.7). The extraterrestrial solar irradiance at the top of the atmosphere is calculated as:

$$S_0 = 1367 \times (1 + 0.033 \times \cos(2\pi \frac{\mathrm{DOY}}{365}) \quad \text{(S3)}$$

where DOY is the day of the year and 1367 W/m^2 is the solar constant. The cosine of the solar zenith angle is computed using:

$$\cos(\theta) = (\sin(\phi) \times \sin(\delta)) + (\cos(\phi) \times \cos(\delta) \times \cos(h)) \quad \text{(S4)}$$

where: ϕ is the latitude in radians, δ is the solar declination angle in radians, and h is the solar hour angle in radians. The solar declination angle is given by:

$$\delta = 23.45\sin(\frac{360(284+\mathrm{DOY})}{365}) \quad \text{(S5)}$$

The hour angle h depends on the local solar time (in decimal hours) and is calculated as:

$$h = 15(Solar\ Time - 12) \quad \text{(S6)}$$

To correct for solar time, we accounted for both longitude and the Equation of Time (EoT, the difference between apparent solar time and mean solar time):

$$Solar\ Time = \mathrm{Clock\ Time} + (\frac{(4(\lambda \mathrm{std} - \lambda) + E_o \mathrm{T})}{60}) \quad \text{(S7)}$$

$$E_oT = 9.87\sin(2\mathrm{B}) - 7.53\cos(\mathrm{B}) - 1.5\sin(\mathrm{B}) \quad \text{(S8)}$$

$$B = 360\frac{DOY-81}{365} \quad \text{(S9)}$$

where:

λ_{std} is the standard meridian for the time zone (in degrees), λ is the local longitude (in degrees), and Clock Time is the local time of day in decimal hours.

Date	Site	Sensor	Start Time (local time)	End Time (local time)	Mean air temp (during flight) [°C]	Stdev air temp (during flight) [°C]	Mean SW_{in} [W/m^2]	Stdev SW_{in} [W/m^2]	Sky Condition	Field camera snow depth (cm)	Judd mean snow depth (cm)	Lidar mean snow depth (cm)
2020/12/23	TF	P4	9:26:00	11:10:00	-1.05	0.48	304.76	38.26	Partly Cloudy	7	9.21	12.8
2021/01/25	TF	P4	10:43:00	11:40:00	-1.86	0.56	428.25	12.55	Cloudy	0	0	No data
2021/02/20	TF	P4	12:04:00	12:44:00	-1.1	0.28	479.63	132.73	Cloudy	20	17.4	24.5
2021/02/23	TF	P4	12:16:00	12:55:00	5.01	0.23	541.13	144.44	Mostly Clear	15	13.8	17.6
2021/02/24	TF	P4	10:41:00	11:20:00	7.55	0.24	590.63	18.59	Clear	10	11.5	13.3
2021/02/26	TF	P4	11:57:00	12:38:00	0.16	0.18	632.75	3.41	Cloudy	7	9.06	8.7
2021/02/28	TF	P4	12:21:00	13:01:00	5.64	0.09	261.63	16.71	Clear	7	9.56	12.5
2021/03/01	TF	P4	16:37:00	17:16:00	5.36	0.16	29.5	17.02	Cloudy	4	7.72	No data
2021/03/03	TF	P4	12:00:00	12:39:00	3.24	0.34	459.63	177.73	Partly Cloudy	3	7.25	5.4
2021/03/07	TF	P4	11:25:00	12:06:00	-2.1	0.25	679.33	2.74	Clear	0	6.38	4.5
2021/03/10	TF	P4	13:50:00	14:34:00	7.84	0.17	541.67	27.6	Clear	0	3.23	No data
2021/03/11	TF	P4	15:12:00	15:51:00	18.89	0.35	265.13	62.83	Clear	0	1.65	0
2021/04/02	TF	P4	14:19:00	14:58:00	2.49	0.21	406.5	94.09	Clear	0	0	No data
2022/01/12	TF	P4	14:47:00	15:26:00	0.43	0.09	19.5	10.07	Clear	4	4.2	No data
2022/01/26	TF	P4	12:50:00	13:32:00	-6.03	0.18	490.11	15.76	Clear	0	0	No data
2024/01/18	KF	P4	13:39:00	14:43:00	-3.25	0.1	162.31	42.14	Partly Cloudy	8	6.4	No data
2024/01/23	KF	P4	14:26:00	15:17:00	3.21	0.03	86.1	23.04	Cloudy	6	6.7	No data
2024/01/27	KF	P4	13:46:00	14:26:00	3.4	0.16	94.25	17.3	Mostly Clear	4	4.6	No data
2024/02/06	KF	P4	14:36:00	15:34:00	3.69	0.14	259.45	40.05	Clear	4	5.4	No data
2024/02/08	KF	P4	13:19:00	13:59:00	6.25	0.14	436	17.19	Clear	2	3.8	No data
2024/02/12	KF	P4	15:40:00	16:27:00	6.12	0.8	80.9	59.04	Partly Cloudy	0	0	No data
2024/02/26	KF	P4	10:45:00	11:25:00	5.34	0.88	491.11	139	Mostly Clear	0	0	No data
2024/04/05	KF	P4	15:16:00	16:02:00	5.61	0.13	95.78	22.5	Cloudy	15	11.9	No data
2024/04/08	KF	P4	14:41:00	15:27:00	16.48	0.76	246.78	96.5	Clear	0	0	No data
2024/12/27	KF	MR	13:25:00	14:10:00	3.5	0.12	165.3	34.01	Cloudy	No data	No data	No data
2025/01/13	KF	P4	15:38:00	16:31:00	0.86	0.3	0	0	Cloudy	No data	No data	No data
2025/02/03	KF	MR	12:15:00	13:00:00	2.81	0.17	356.3	8.43	Partly Cloudy	No data	No data	16.6
2025/02/19	KF	MR	12:25:00	13:15:00	-4.84	0.29	424.27	8.67	Mostly Clear	No data	No data	40.7
2025/03/09	KF	MR	14:35:00	15:20:00	4.35	0.24	192.9	27.29	Partly Cloudy	No data	No data	6.9
2025/03/10	KF	MR	16:45:00	17:25:00	12.31	0.28	196.56	44.89	Mostly Clear	No data	No data	4.3

Table S2, Summary of snow and meteorological condition at the UAS survey dates

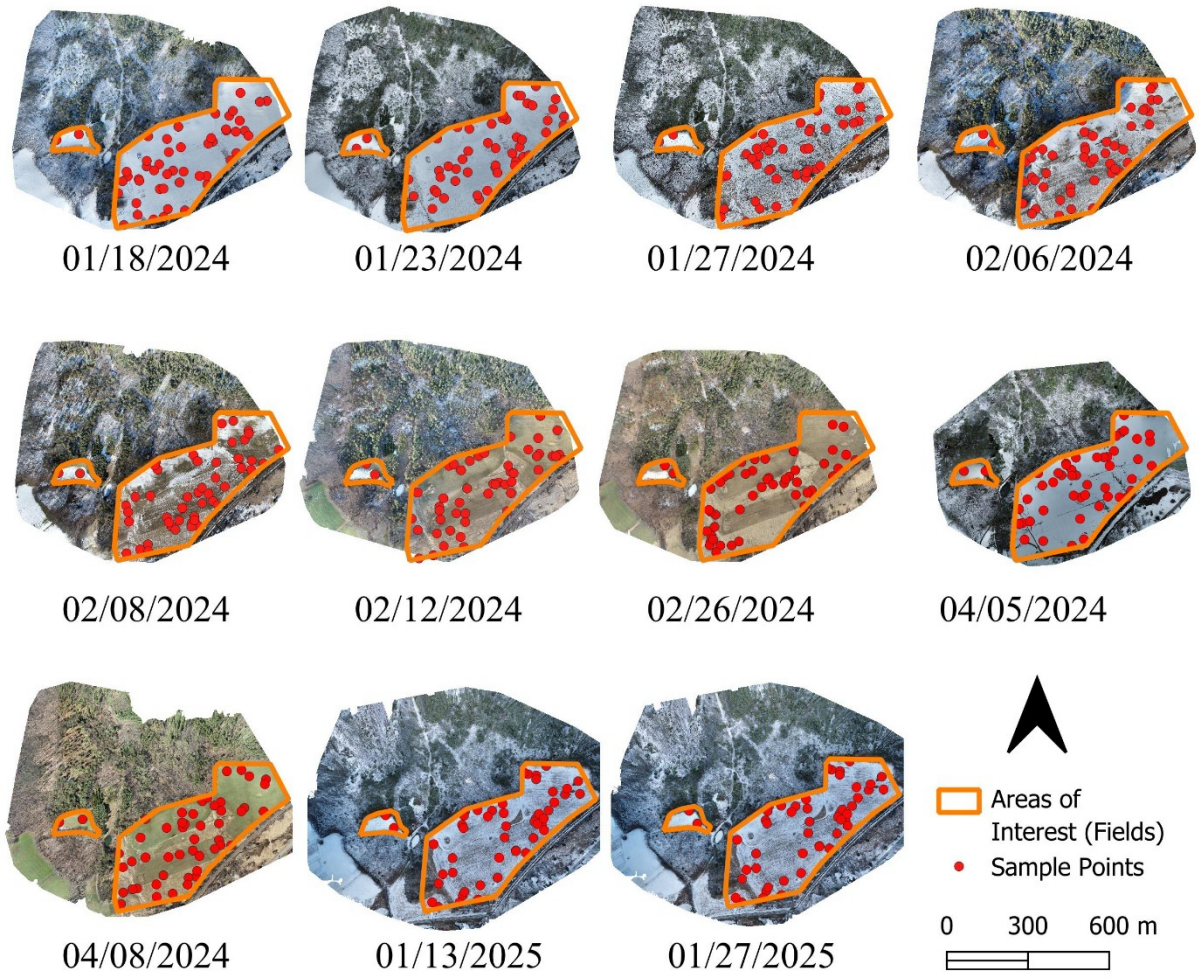


Figure S3. RGB orthomosaics of Kingman Farm acquired with the Phantom 4. Survey dates are shown below each image. Areas of interest are outlined in orange. Random sample points are shown as red dots.

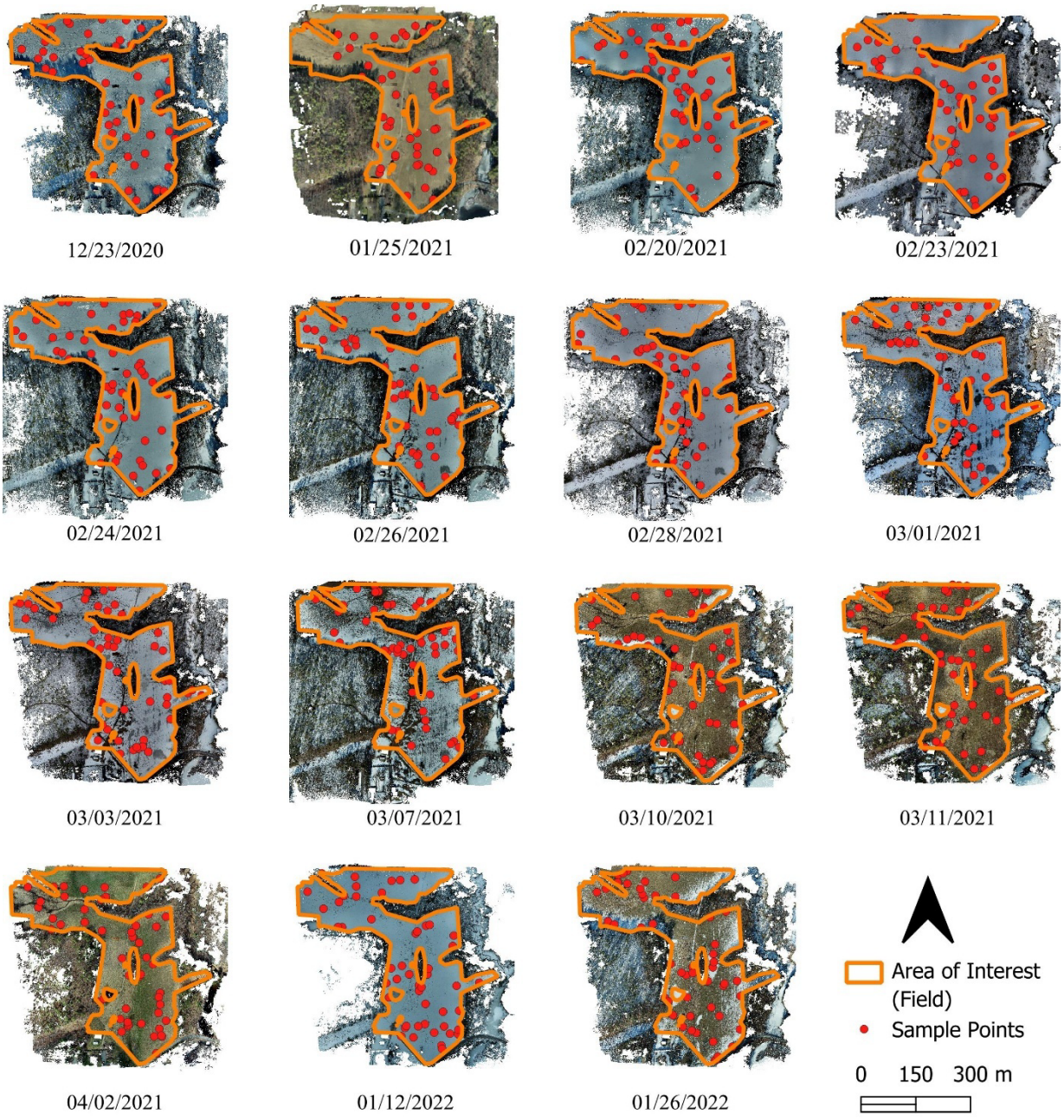


Figure S4. RGB orthomosaics of Thompson Farm acquired with the Phantom 4. Survey dates are shown below each image. Areas of interest are outlined in orange. Random sample points are shown as red dots.

Details on Greenvalley LiAir v70

The Greenvalley LiAir v70 and the Phoenix miniRanger3 both have an integrated Sony A5100 camera as part of the sensor payload. The Sony A5100 has a 23.5 x 15.6 mm back illuminated APS-C CMOS sensor containing 24 megapixels. During operation, a fixed shutter speed of

1/1000s and a fixed aperture setting of f/5.6 were used. Automatic exposure adjustments were made solely by changing the ISO setting. The pattern light metering mode with no exposure bias was used to determine the appropriate ISO adjustment for each image capture. The fixed high shutter speed and large aperture opening prevents image blurring. Because this UAS is primarily lidar payloads, image overlap capture is not as easily customizable as with the Phantom 4 RTK. For this study, images were collected at a time interval of 2 seconds, resulting in a forward overlap of ~80%. Likewise, flightline spacing was chosen to ensure 70% lidar swath overlap, resulting in ~80% image side overlap. Flightlines were made using the UgCS flight planning software. A DEM was referenced within UgCS to ensure a consistent flight altitude was maintained throughout each flight. Flights with the v70 were conducted at an altitude of 50 m, whereas miniRanger3 flights were conducted at 80 m. The resulting GSD was ~2 cm and ~3 cm, respectively.

Table S3. Mean balanced accuracies for different static blue band thresholds, averaged over five trials each. The optimal threshold (135) is bolded.

Threshold	Mean Balanced Accuracy
95	0.732
105	0.769
115	0.797
127	0.828
135	**0.849**
145	0.825

Table S4 - Pairwise Wilcoxon tests on balanced accuracy with FDR correction

Classifier 1	Classifier 2	Wilcoxon statistic	raw p-value	FDR-corrected p-value	Significant at alpha=0.05
RF	SVM	14.0	0.193359	0.214844	False
RF	SVM Blue	0.0	0.001953	0.003255	True
RF	MLE	19.0	0.431641	0.431641	False
RF	Static Blue	0.0	0.001953	0.003255	True
SVM	SVM Blue	0.0	0.001953	0.003255	True
SVM	MLE	9.0	0.121094	0.151367	False
SVM	Static Blue	0.0	0.001953	0.003255	True
MLE	SVM Blue	0.0	0.001953	0.003255	Tue
MLE	Static Blue	0.0	0.001953	0.003255	True
SVM Blue	Static Blue	4.0	0.013672	0.019531	False

Table S5 - Pairwise Wilcoxon tests on F1 score with FDR correction

Classifier 1	Classifier 2	Wilcoxon statistic	raw p-value	FDR-corrected p-value	Significant at alpha=0.05
RF	SVM	11.0	0.105469	0.117188	False
RF	SVM Blue	0.0	0.001953	0.003255	True
RF	MLE	9.0	0.064453	0.080566	False
RF	Static Blue	0.0	0.001953	0.003255	True
SVM	SVM Blue	0.0	0.001953	0.003255	True
SVM	MLE	12.0	0.250000	0.250000	False
SVM	Static Blue	0.0	0.001953	0.003255	True
MLE	SVM Blue	0.0	0.001953	0.003255	True
MLE	Static Blue	0.0	0.001953	0.003255	True
SVM Blue	Static Blue	9.0	0.064453	0.080566	False

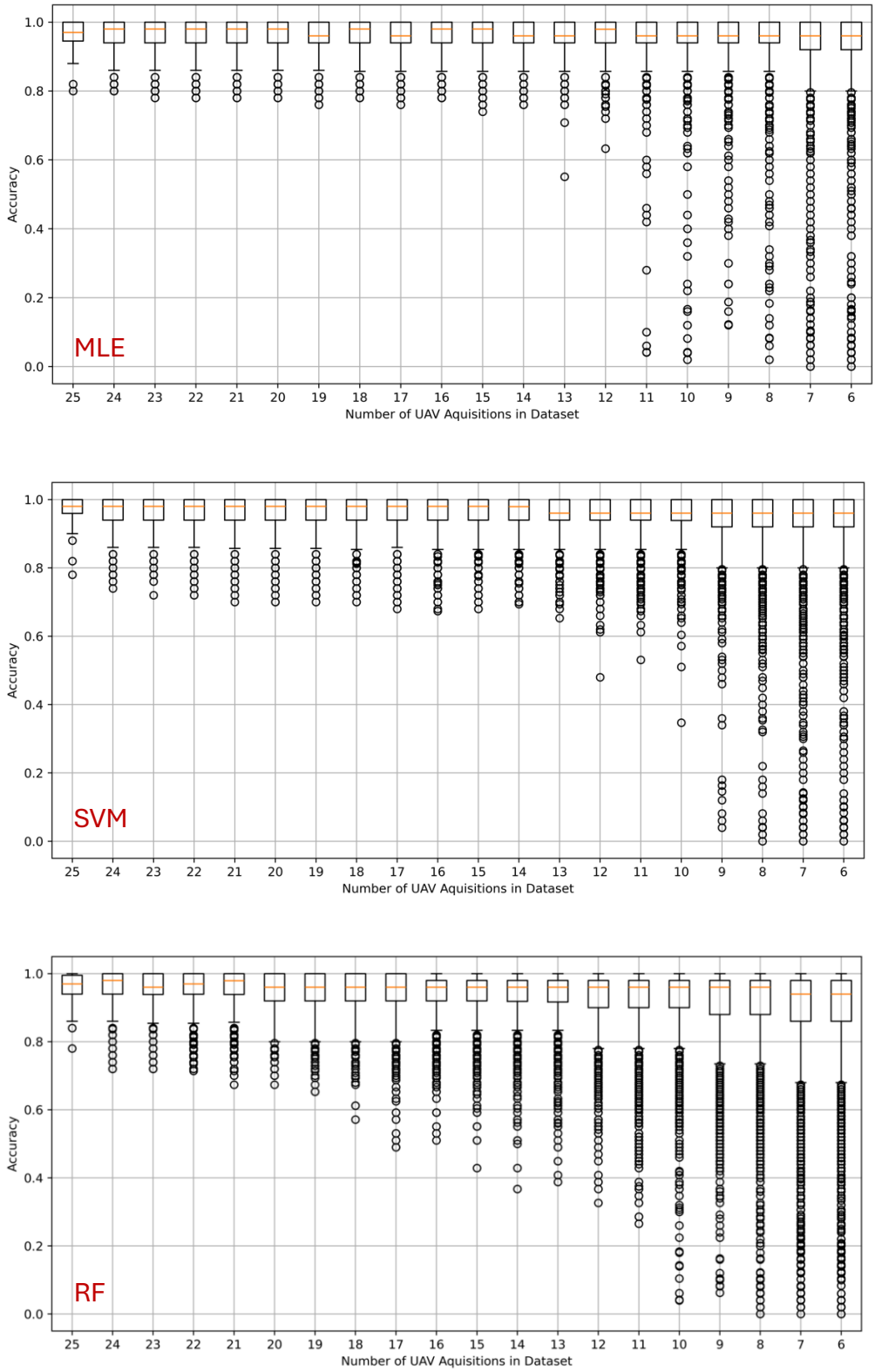


Figure S5. Accuracy of the three classifiers on left-out orthomosaics, shown in relation to the number of orthomosaics included in the dataset. Top is MLE, middle is SVM, and bottom is RF.

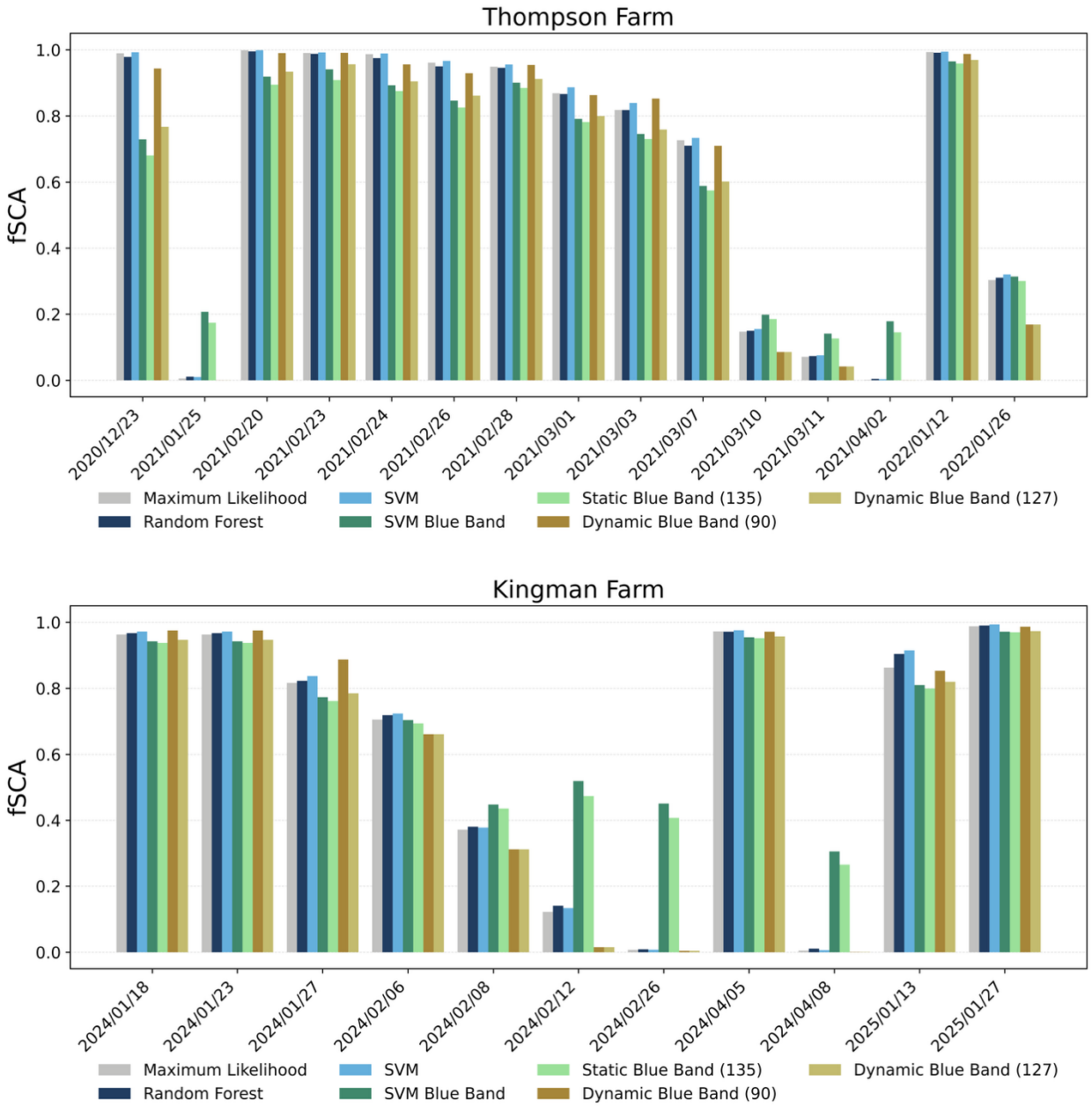


Figure S6. Comparison of factional snow-covered area (fSCA) across different SCA classification methods for each UAV acquisition date at two study sites. The fSCA is calculated as the proportion of pixels classified as snow relative to the total valid pixels in the orthomosaic.

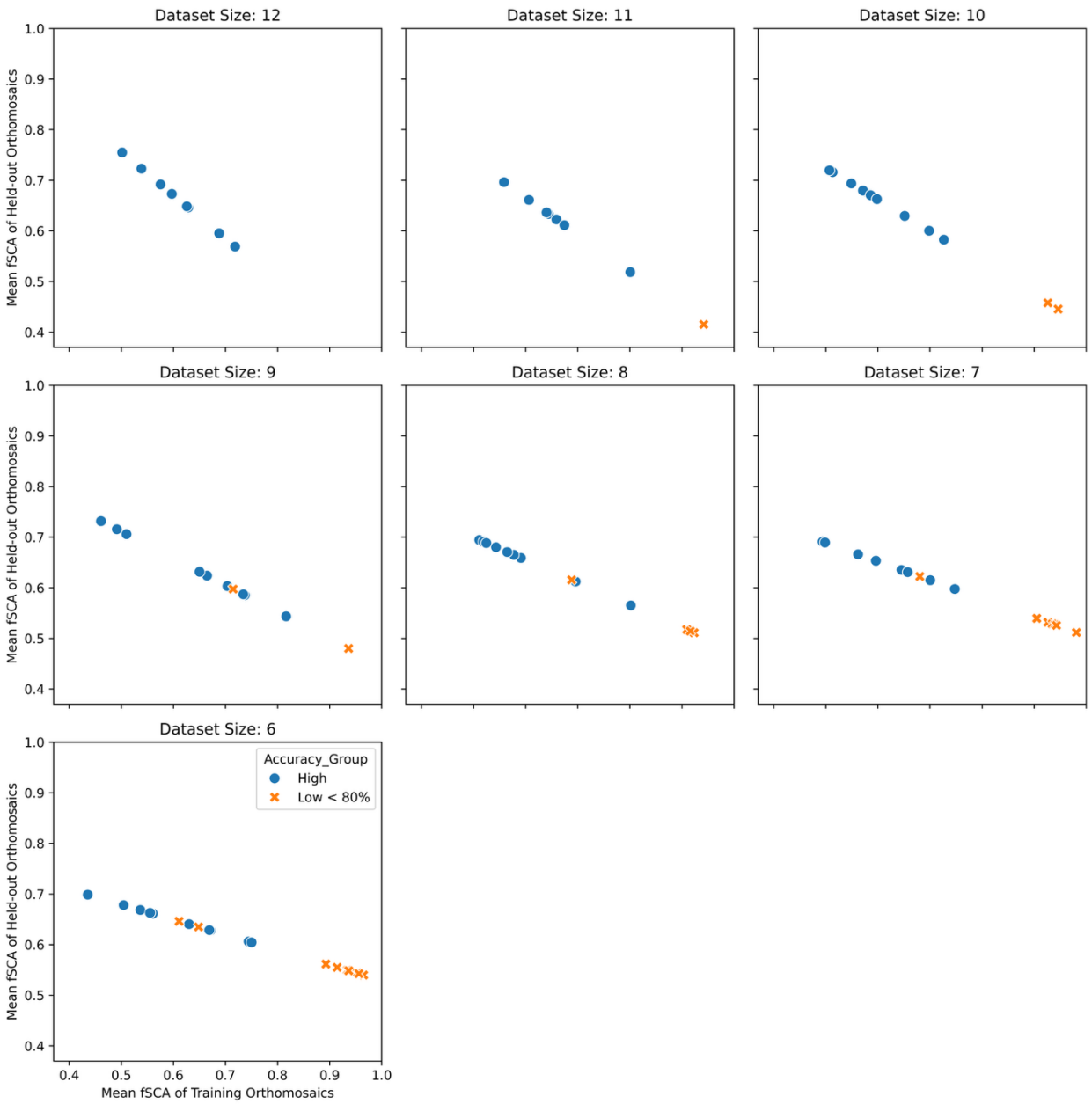


Figure S7. Mean fSCA of orthomosaics within training vs. Mean fSCA of held-out orthomosaics for the 20 combinations (10 highest and 10 lowest (<80%) accuracy) for the MLE classifier. Blue dots represent high-accuracy combinations; orange dots represent low-accuracy combinations. The individual plots differ by the number of orthomosaics in the training dataset. Training dataset sizes of 10, 11, and 12 did not have any held-out datasets with accuracy values < 80%.

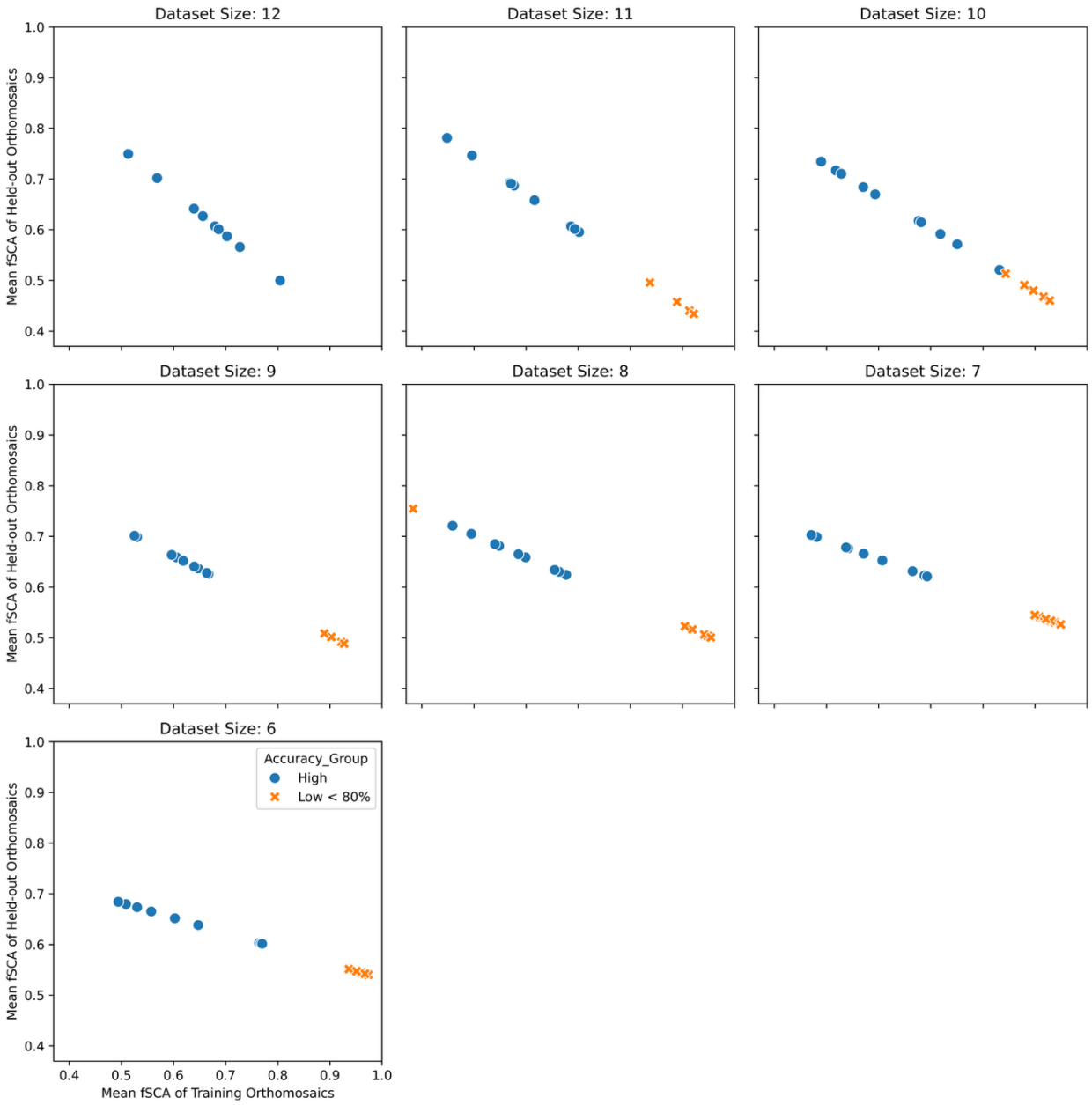


Figure S8. Mean fSCA of orthomosaics within training vs. Mean fSCA of held-out orthomosaics for the 20 combinations (10 highest and 10 lowest (<80%) accuracy) for the RF classifier. Blue dots represent high-accuracy combinations; orange dots represent low-accuracy combinations. The individual plots differ by the number of orthomosaics in the training dataset. Training dataset sizes of 10, 11, and 12 did not have any held-out datasets with accuracy values < 80%.

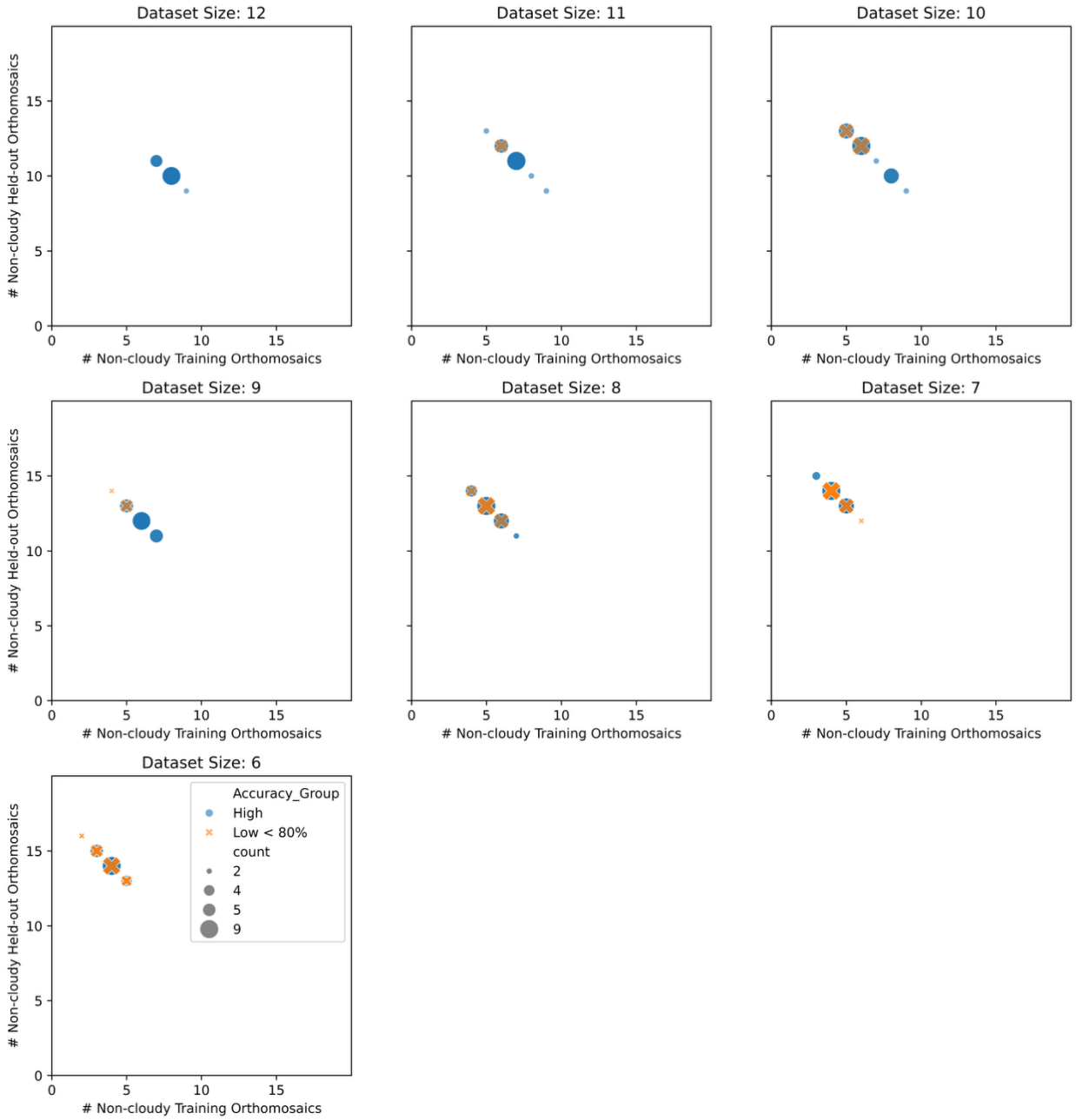


Figure S9. Number of non-cloudy orthomosaics within training set VS. Number of non-cloudy orthomosaics within held-out set for the 20 combinations (10 highest and 10 lowest (<80%) accuracy) for the MLE classifier. Blue dots represent high-accuracy combinations; orange dots represent low-accuracy combinations

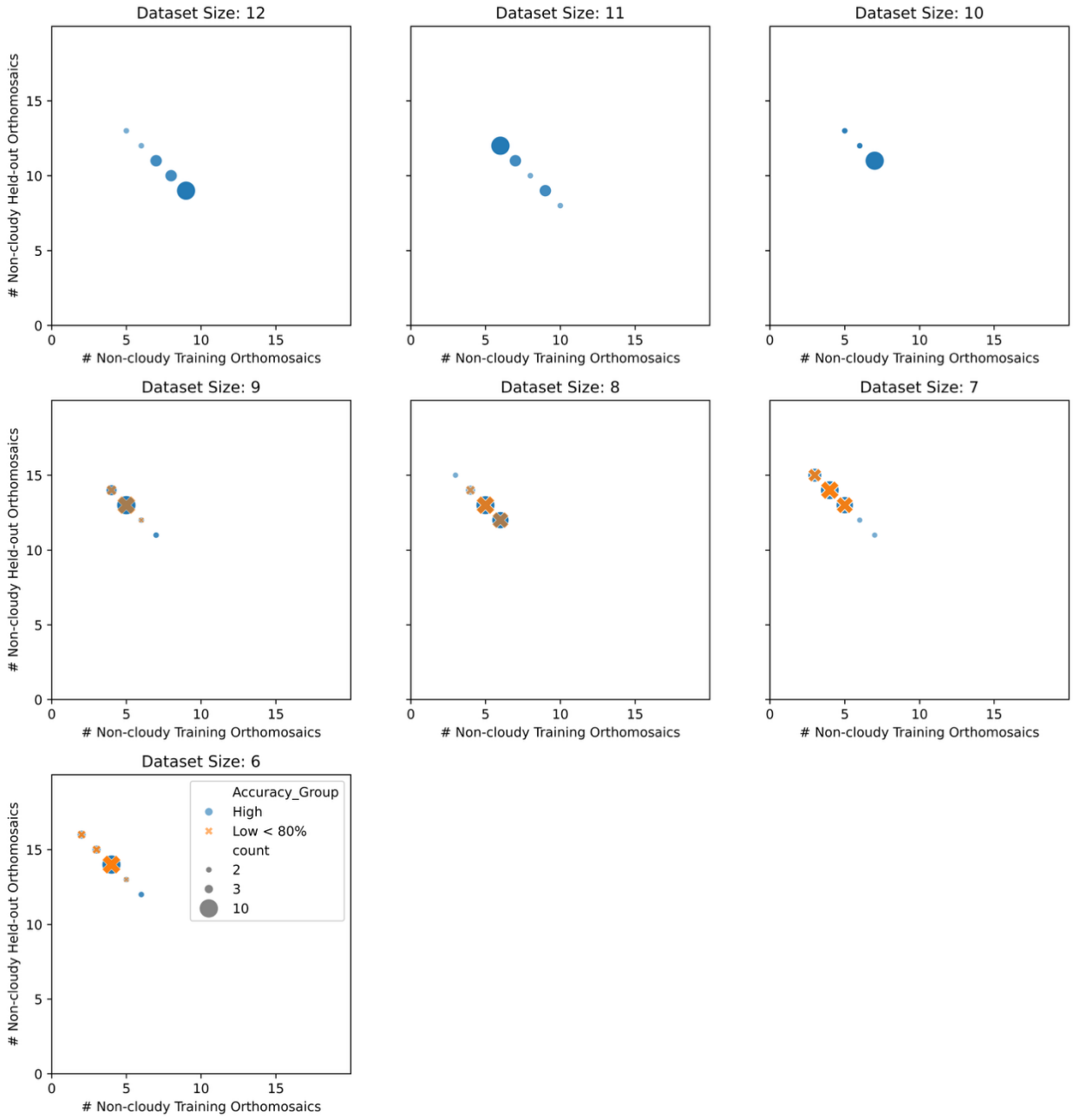
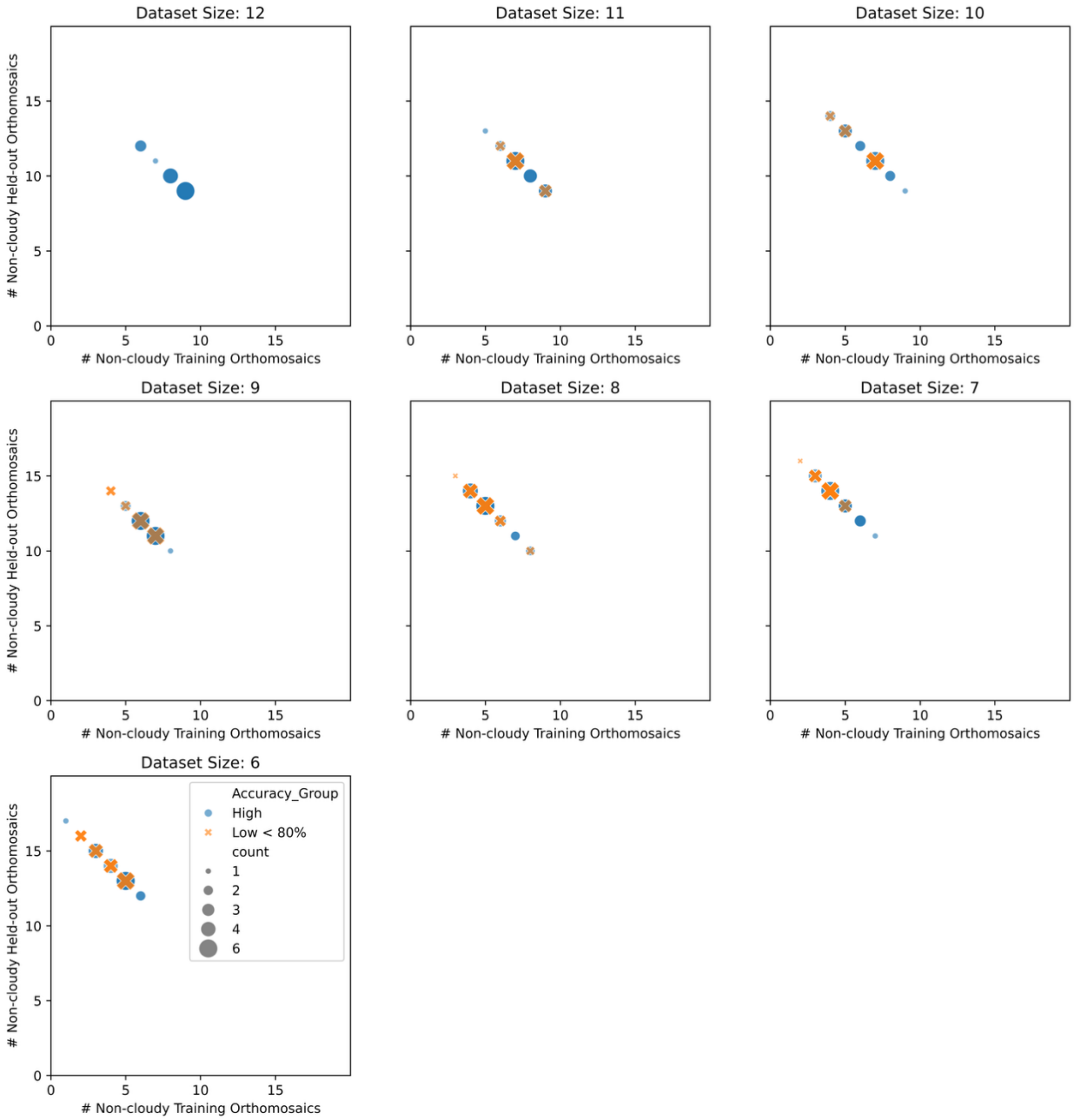
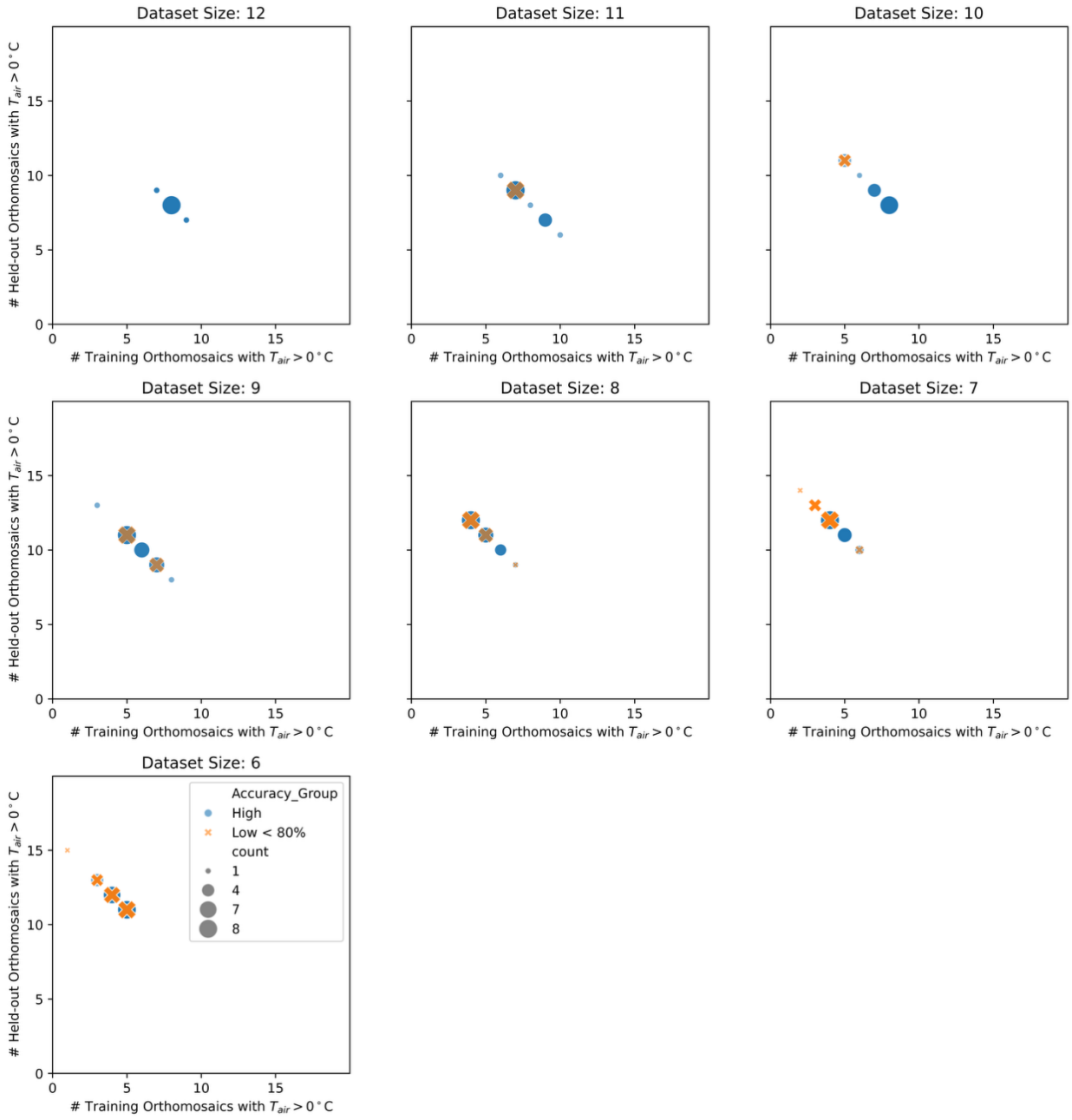


Figure S10. Number of non-cloudy orthomosaics within training set VS. Number of non-cloudy orthomosaics within held-out set for the 20 combinations (10 highest and 10 lowest (<80%) accuracy) for the SVM classifier. Blue dots represent high-accuracy combinations; orange dots represent low-accuracy combinations

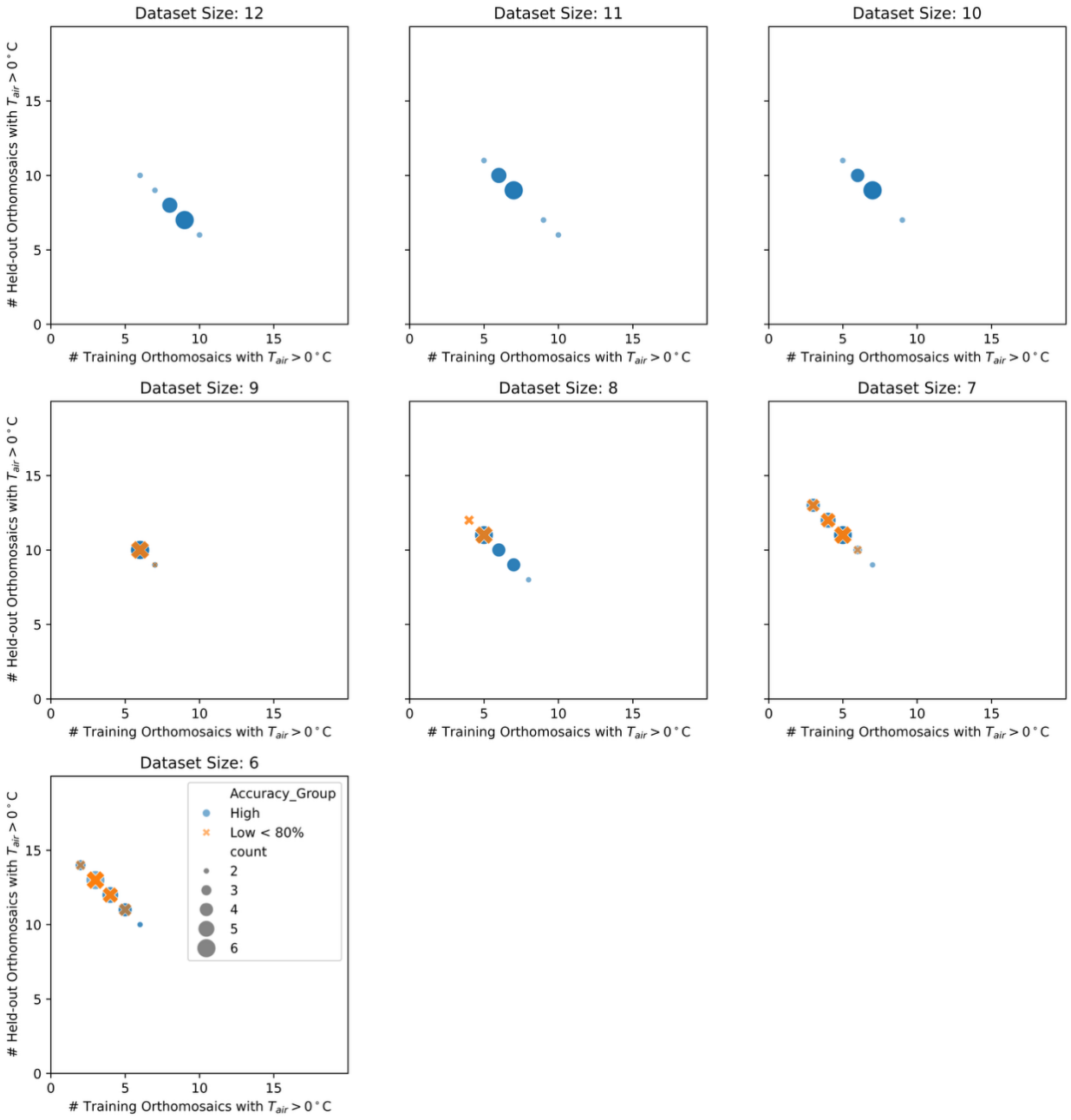


115 **Figure S11.** Number of non-cloudy orthomosaics within training set VS. Number of non-cloudy orthomosaics within held-out set for the 20 combinations (10 highest and 10 lowest (<80%) accuracy) for the RF classifier. Blue dots represent high-accuracy combinations; orange dots represent low-accuracy combinations



120

Figure S12. Number of days with air temperature above freezing within training set VS. Number of days with air temperature above freezing within held-out set for the 20 combinations (10 highest and 10 lowest (<80%) accuracy) for the MLE classifier. Blue dots represent high-accuracy combinations; orange dots represent low-accuracy combinations



125

Figure S13. Number of days with air temperature above freezing within training set VS. Number of days with air temperature above freezing within held-out set for the 20 combinations (10 highest and 10 lowest (<80%) accuracy) for the SVM classifier. Blue dots represent high-accuracy combinations; orange dots represent low-accuracy combinations

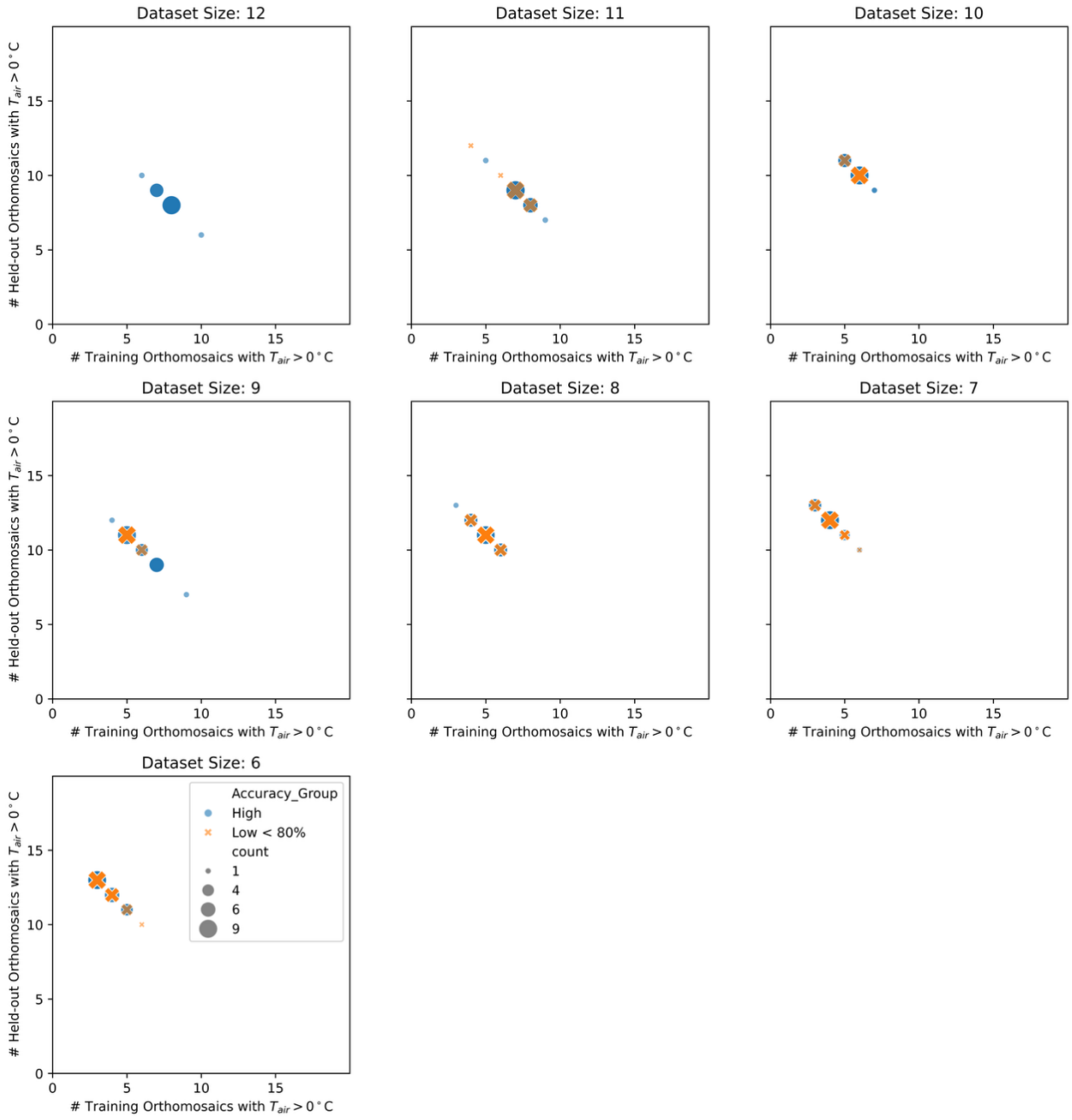


Figure S14. Number of days with air temperature above freezing within training set VS. Number of days with air temperature above freezing within held-out set for the 20 combinations (10 highest and 10 lowest (<80%) accuracy) for the RF classifier. Blue dots represent high-accuracy combinations; orange dots represent low-accuracy combinations

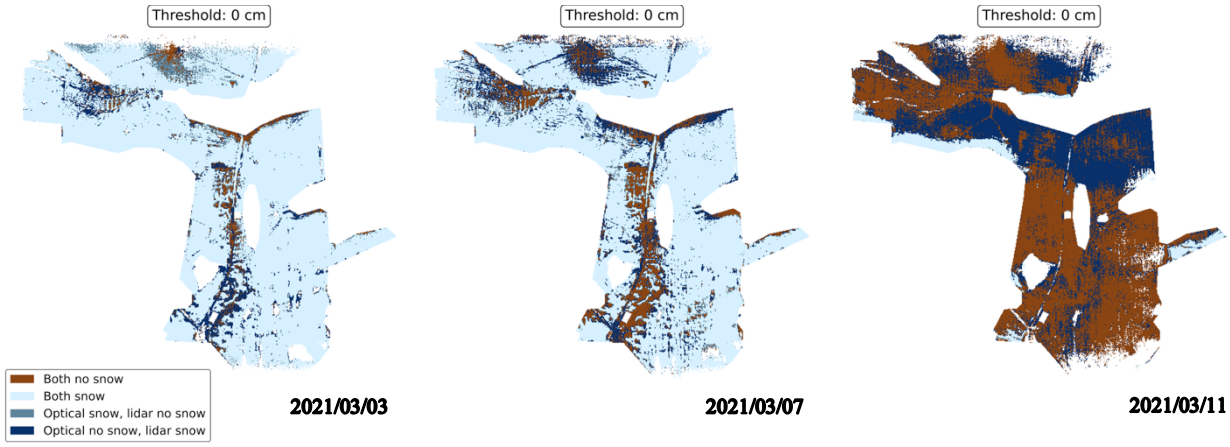


Figure S15. Comparison between optical and lidar-derived snow cover maps during melt phase

Table S6. Confusion matrix for dynamic thresholding approach with minimum threshold of 127

Date	Site	TN	FP	FN	TP
2020/12/23	TF	0	0	15	35
2021/01/25	TF	50	0	0	0
2021/02/20	TF	0	0	2	48
2021/02/23	TF	0	0	2	48
2021/02/24	TF	0	0	6	44
2021/02/26	TF	0	0	4	46
2021/02/28	TF	2	0	1	47
2021/03/01	TF	5	0	3	42
2021/03/03	TF	5	0	8	37
2021/03/07	TF	19	0	7	24
2021/03/10	TF	45	0	3	2
2021/03/11	TF	45	0	3	2
2021/04/02	TF	50	0	0	0
2022/01/12	TF	2	0	0	48
2024/01/18	KF	0	1	0	49
2024/01/23	KF	2	0	0	48
2024/01/27	KF	10	1	1	38
2024/02/06	KF	17	2	5	26
2024/02/08	KF	30	0	6	14
2024/02/12	KF	48	0	1	0
2024/02/26	KF	48	0	0	0
2024/04/05	KF	4	0	2	44
2024/04/08	KF	49	0	1	0
2025/01/27	KF	0	0	8	42

Table S7. Confusion matrix for dynamic thresholding approach with minimum threshold of 90

Date	Site	TN	FP	FN	TP
2020/12/23	TF	0	0	6	44
2021/01/25	TF	50	0	0	0
2021/02/20	TF	0	0	0	50
2021/02/23	TF	0	0	0	50
2021/02/24	TF	0	0	2	48
2021/02/26	TF	0	0	3	47
2021/02/28	TF	2	0	0	48
2021/03/01	TF	5	0	1	44
2021/03/03	TF	4	1	2	43
2021/03/07	TF	16	3	3	28
2021/03/10	TF	45	0	3	2
2021/03/11	TF	45	0	3	2
2021/04/02	TF	50	0	0	0
2022/01/12	TF	0	2	0	48
2024/01/18	KF	0	1	0	49
2024/01/23	KF	2	0	0	48
2024/01/27	KF	7	4	0	39
2024/02/06	KF	17	2	5	26
2024/02/08	KF	30	0	6	14
2024/02/12	KF	48	0	1	0
2024/02/26	KF	48	0	0	0
2024/04/05	KF	3	1	1	45
2024/04/08	KF	49	0	1	0
2025/01/27	KF	0	0	5	45

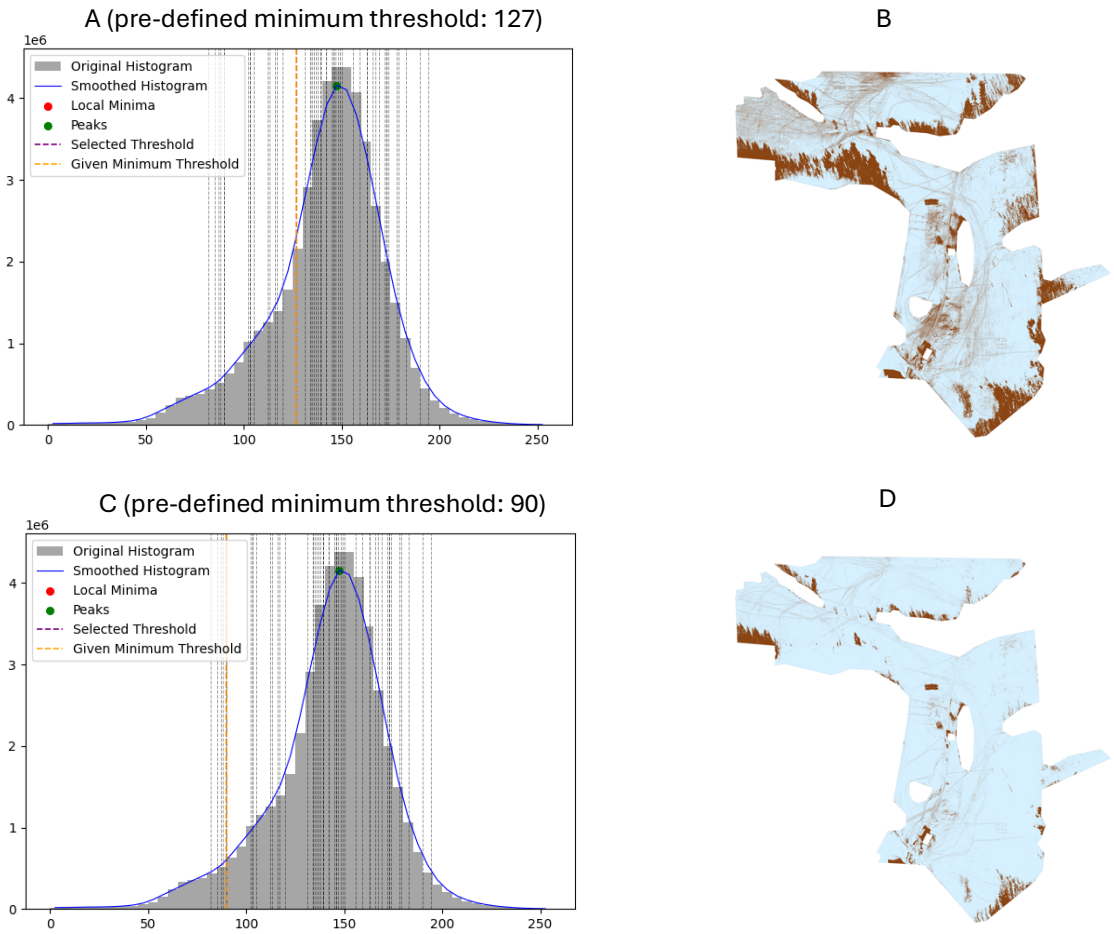


Figure S16. Histogram of blue band intensity (A, C) and the estimated maps based on the selected threshold (B, D) at Thompson Farm on 2020/12/23. The gray bars represent the original histogram of pixel intensities, and the blue line shows the smoothed version. Local minima and peaks are marked in red and green, respectively. The vertical dashed lines indicate: the selected threshold (magenta), the pre-defined minimum threshold (orange), and the blue band intensity values of randomly sampled pixels (gray dotted lines).

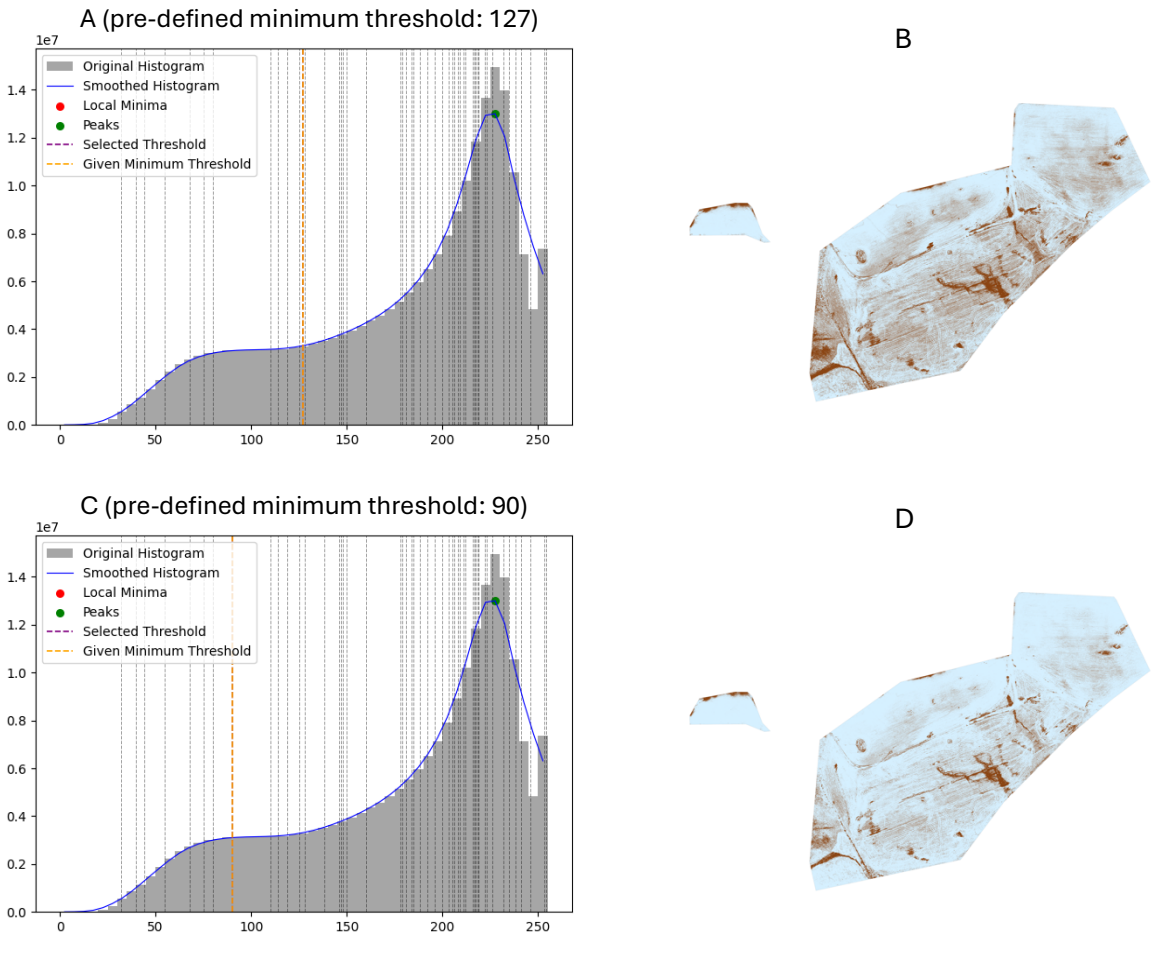


Figure S17. Histogram of blue band intensity (A, C) and the estimated maps based on the selected threshold (B, D) at Kingman Farm on 2024/01/27. The gray bars represent the original histogram of pixel intensities, and the blue line shows the smoothed version. Local minima and peaks are marked in red and green, respectively. The vertical dashed lines indicate: the selected threshold (magenta), the pre-defined minimum threshold (orange), and the blue band intensity values of randomly sampled pixels (gray dotted lines).

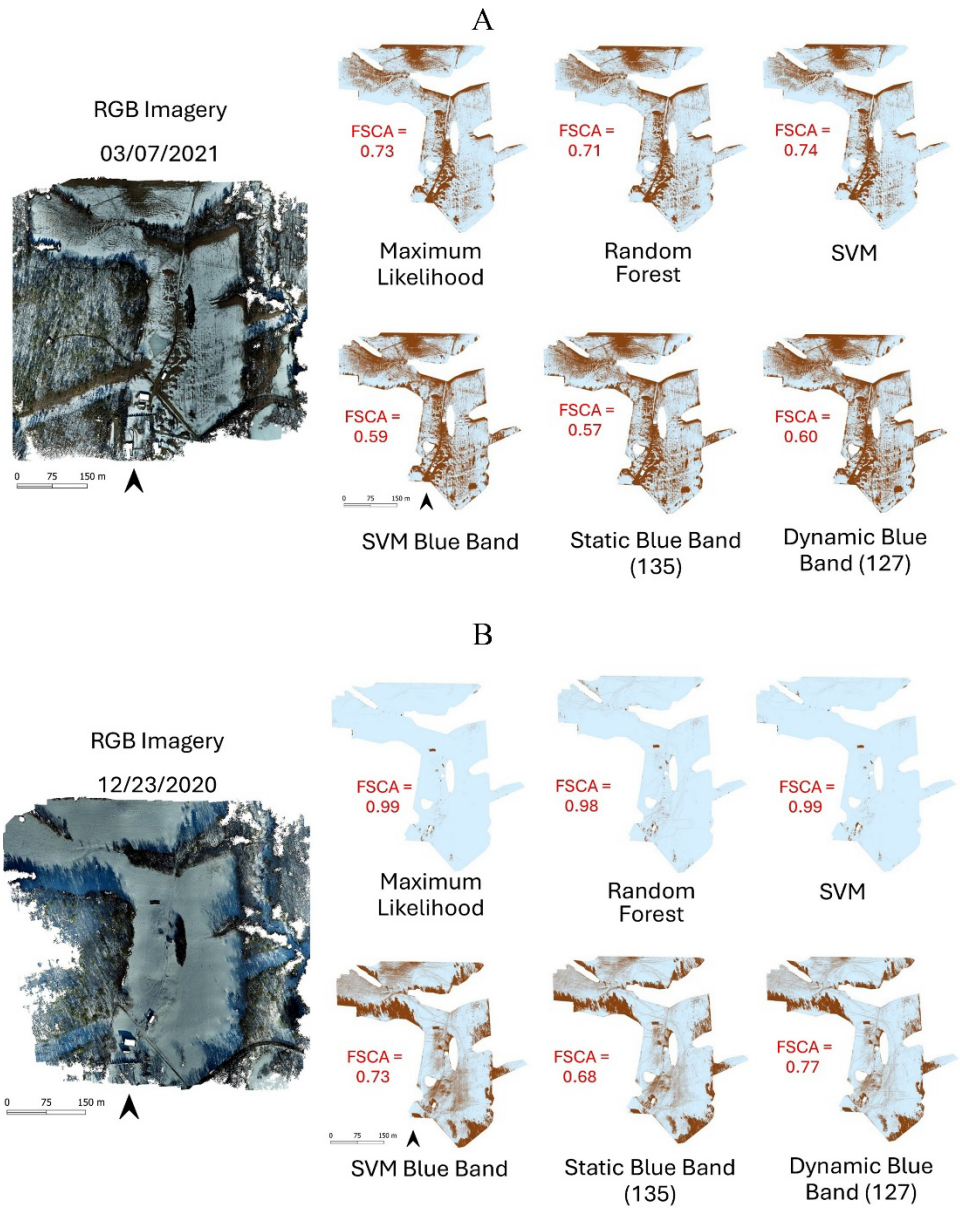


Figure S18. UAS orthomosaics from Thompson Farm on A) March 7th, 2021 and B) December 23rd, 2020 derived and SCA classification using each of the six classifiers. Fractional snow cover (fSCA) is noted for each classifier. Purple circles delineate areas of deep shade on December 23rd, 2020.

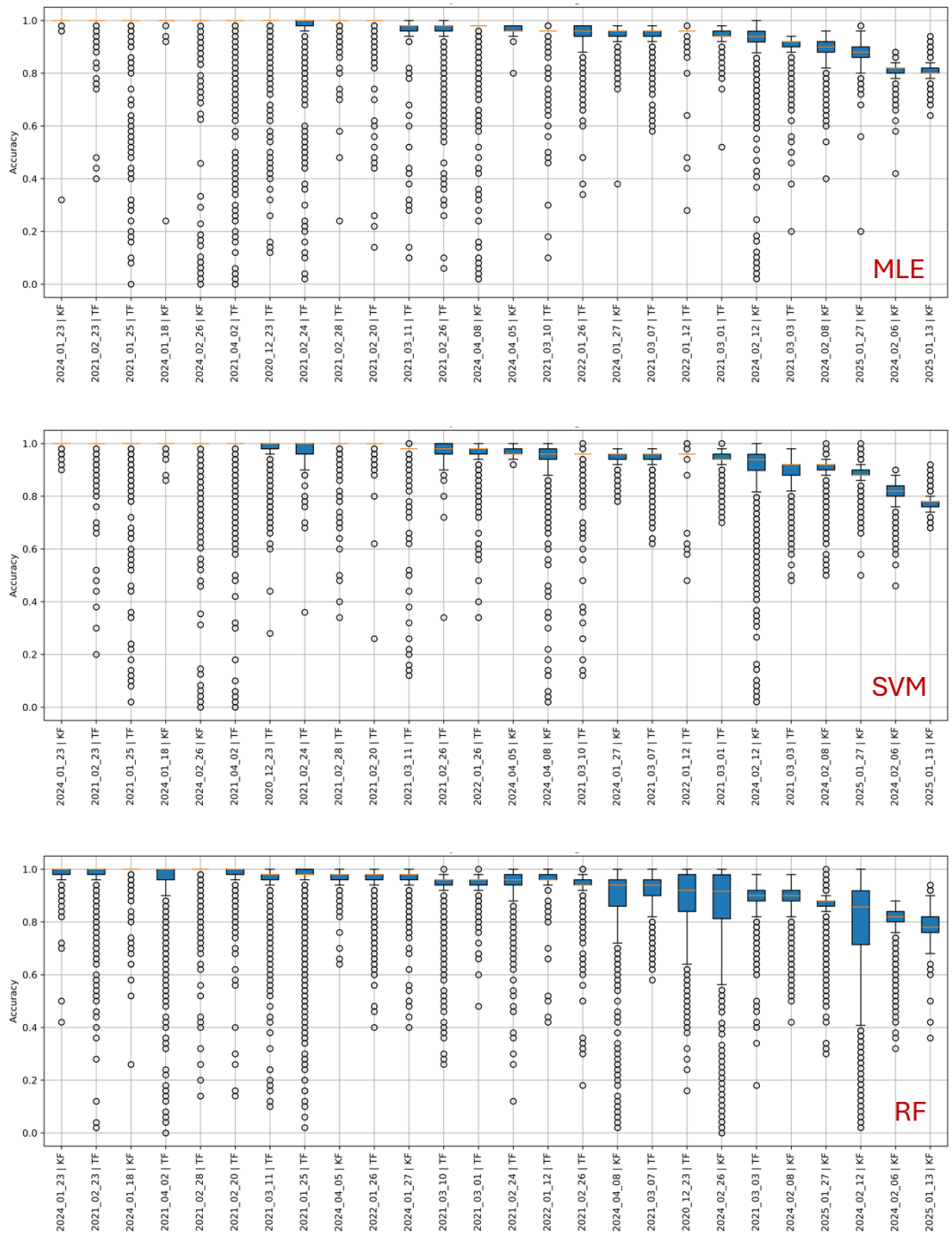
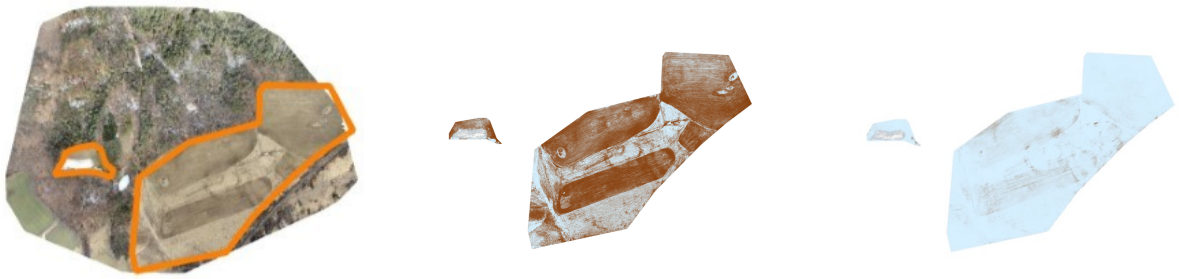


Figure S19. Accuracy of Experiment 4 models on each orthomosaic across all instances in which that orthomosaic was held-out.



(A) (B)

Figure S20. Snow cover maps estimated by random forest classifier, trained based on data from 8 orthomosaics, with 60% accuracy (A) and 1% accuracy (B) on 2024/02/26 KF orthomosaic

SCA Mapping in Forest Gaps:

In this study, we mapped snow cover in forested environments by first identifying and masking tree canopies. Tree canopy masks were generated using an unsupervised clustering approach applied to the orthomosaic imagery. A representative subset of pixels was randomly sampled from each image to capture the range of surface conditions present in the scene. The sampled pixel values were transformed into the CIELAB color space and reduced using principal component analysis (PCA) to improve feature separability and reduce dimensionality. K-medoids clustering was then applied to classify pixels into multiple clusters representing different surface types. The cluster corresponding to tree canopy was identified through visual inspection and used to generate a binary mask that removed forested areas from each orthomosaic. After masking the canopy, 50 validation points were randomly sampled from the remaining gaps between tree canopies and labeled as snow or no snow. The models trained in the open-field experiments presented in this manuscript were then applied to estimate snow cover at these validation points, and their performance was evaluated. An example of the classification of tree canopy and subsequent SCA classification of the ground is shown in the following figure

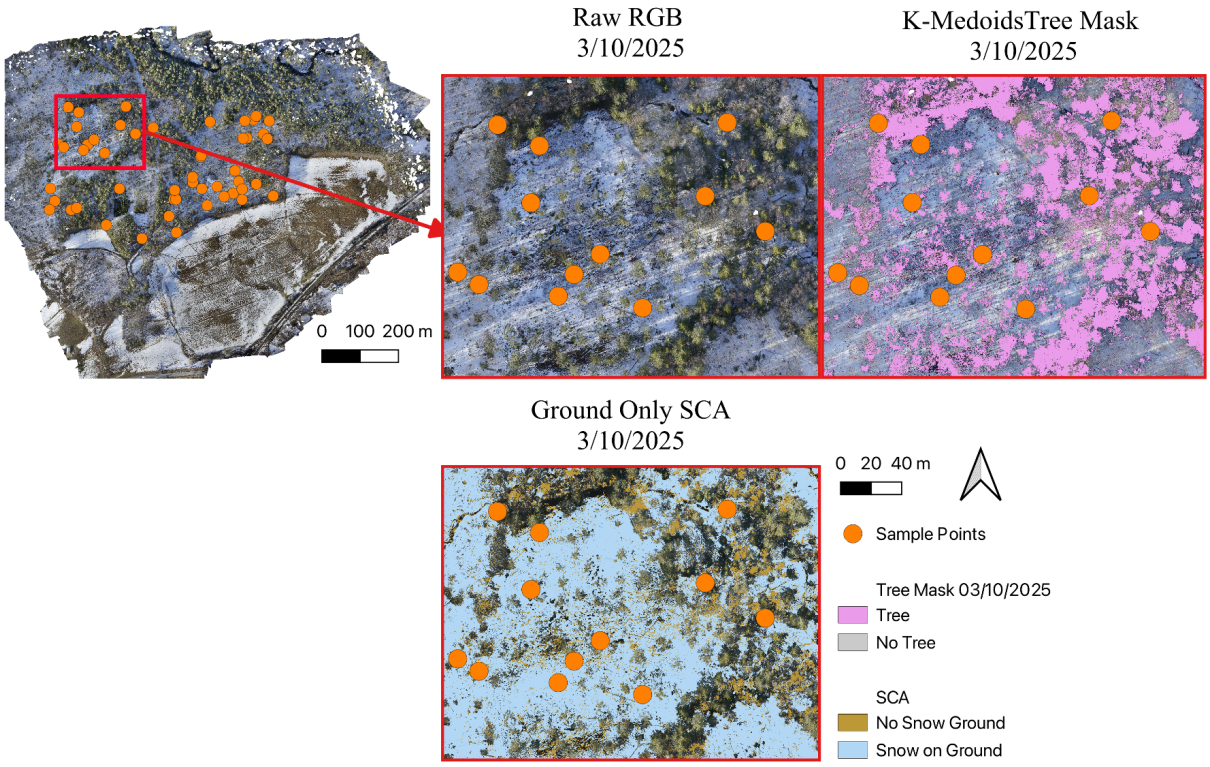


Figure S21. Example of SCA mapping in forest gaps on 10 March 2025 using tree masking derived from K-medoids clustering.